International Journal of Bifurcation and Chaos, Vol. 17, No. 1 (2007) 199–208

POINCARÉ PLANES IN NONLINEAR ELECTRONICS

E. CAMPOS-CANTÓN
Departamento de Físico Matemáticas,
Universidad Autónoma de San Luis Potosí,
SLP, México

J. S. GONZÁLEZ
Universidad Politécnica de San Luis Potosí,
SLP, México

J. URÍAS
Instituto de Física,
Universidad Autónoma de San Luis Potosí,
SLP, México

Received May 5, 2005; Revised January 23, 2006

Details of electronic circuitry to define Poincaré planes in the phase space of nonlinear electronic systems are presented. It allows an experimental setup to capture data at every moment the system's orbit crosses the Poincaré plane. We illustrate how the circuit is used in an experimental setup that allows us (i) to reconstruct bifurcation cascades and to disclose induced first return chaotic maps in a harmonically forced nonlinear oscillator, and (ii) to study bistable switching in Chua's oscillator.

Keywords: Poincaré cross-sections; nonlinear oscillators; bifurcations; bistable switching.

1. Introduction

Poincaré had the idea to put a section of a surface perpendicular to the flow generated by a system of differential equations and then study the sequence $P_0, P_1, \ldots, P_n, P_{n+1}, \ldots$ of points where an orbit successively intersects the section. The crossing of the flow defines a (first return) mapping of the cross-section into itself, such that point P_{n+1} is the image of point P_n. A methodic application of Poincaré's idea has played a prominent role in the study of dynamical systems.

In the period 1950–1960 methods of pointwise mappings (the first return maps of Poincaré) for the study of (theoretical and technical) nonlinear oscillations were developed under the guidance of Yu. I. Neimark.[1] Using these methods, "stochastic self-sustained oscillations" were found to exist by Neimark's team (about ten years earlier than the Lorenz attractor, in 1963) [Diner, 1992]. The strange attractor is the mathematical form of stochastic self-sustained (chaotic) oscillations.

Progress in the study of nonlinear dynamical systems in the second half of the past century was boosted by the experimental study of chaotic oscillations in nonlinear electronic systems,

[1]Methods and paradigms of nonlinear physics were developed in the Gorki school, initiated in the 1930's by Andronov. See [Diner, 1992].

lately in the area of chaos synchronization.[2] For instance, a theoretical framework for multimodal synchronization of chaos was presented and confirmed experimentally in [Campos *et al.*, 2004]. The experimental methods in [Campos *et al.*, 2004] make an essential use of Poincaré planes and of the maps induced on it by the flow.

In the present article, we describe an electronic circuit that allows an experimental setup to capture the points in phase space where a *system*'s orbit intersects a Poincaré plane. As the *system* we choose either Chua's circuit [Madan, 1993] or a nonlinear electronic oscillator with a rich variety of attractors in $\mathbb{R}^3$ [Rulkov, 1996]. The circuit for Poincaré planes is described in Sec. 2. It has adjustable parameters that allow us to handle the position of the plane in phase space. In Sec. 3.1 we illustrate how to follow a cascade of bifurcations by using the circuit for Poincaré planes. The method yields accurate estimates of bifurcation points out of experimental data. As a first example in Sec. 3.2 we consider the oscillator forced by a sinusoidal external signal with an amplitude that puts the oscillator close to a Hopf–Andronov bifurcation point. We describe an experimental setup that makes use of the circuit for Poincaré planes to capture data and extract from it, in a homeomorphic way, a map of the circle and estimate its rotation number. Section 3.2 is concluded by considering the oscillator in a Rössler-type attractor. The circuit for Poincaré planes allows us here to show that orbits around the attractor distribute according to the dynamics of surjective (i.e. fully chaotic) logistic maps. In Sec. 4 Chua's circuit is considered with electronic components that put it in a (nonchaotic) bistable mode. A sinusoidal external signal of amplitude λ is applied. We found that there exists a threshold value of the amplitude, λ_*, for bistable switching induced by the external signal. By collecting experimental data by means of the circuit for Poincaré planes an accurate estimate of λ_* is feasible. Finally, in Sec. 5 we discuss how the circuit for Poincaré planes in $\mathbb{R}^3$ can be extended to deal with higher dimensional electronic systems.

2. A Circuit for Poincaré Planes

We will frame the description of the circuit for Poincaré planes in the phase space of third-order nonlinear oscillators (two examples are considered in Secs. 3 and 4). In this way Poincaré planes are just "familiar planes" in $\mathbb{R}^3$. The attractor of a nonlinear oscillator, reconstructed from experimental data, is shown in Fig. 1 along with a Poincaré plane. For the particular forms of attractors we are dealing with, it is convenient to use three control parameters (m, q_1 and q_2) for the Poincaré plane,

$$\Sigma := \{x = (x_1, x_2, x_3) \in \mathbb{R}^3 : \; x_2 = mx_1 + (q_2 - mq_1)\}.$$

The plane Σ is perpendicular to the x_1–x_2 plane and intersects it at the line specified by $x_2 = mx_1 + (q_2 - mq_1)$. Parameters behave as follows. Location of the plane Σ is determined by point $Q = (q_1, q_2, 0)$ and its orientation is determined by slope m of the intersecting line. Point Q is indicated by a dot in Fig. 1.

We look for an experimental setup that captures the value of all state variables of a third-order electronic oscillator at each time the orbit in phase space intersects the Poincaré plane, which is determined by the parameters m, Q. The required device for that, considered as a black box, must have knobs to set m and Q, have inputs for the state variables and yield out a squared waveform, $s(t)$, with a rising edge at the time the orbit intersects the Poincaré plane in the positive direction and a negative edge when the orbit intersects the plane the other way around. This idea is shown in Fig. 2

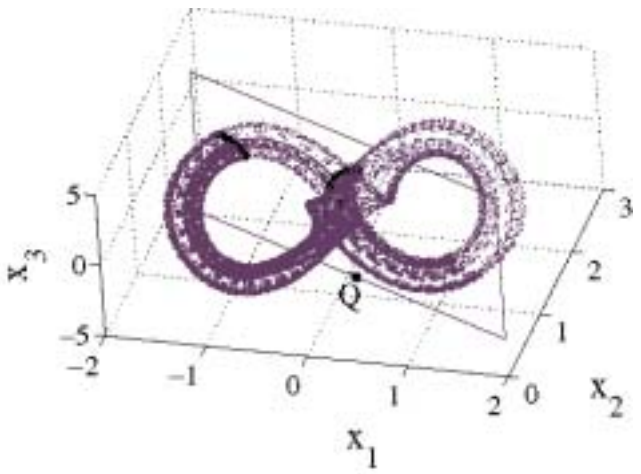

Fig. 1. Attractor of the nonlinear oscillator Fig. 5 (parameter values are those in the first column of the table that accompanies the schematics). The attractor is being cut by a Poincaré plane.

[2]For an overview see [Rulkov, 1996] and [Madan, 1993].

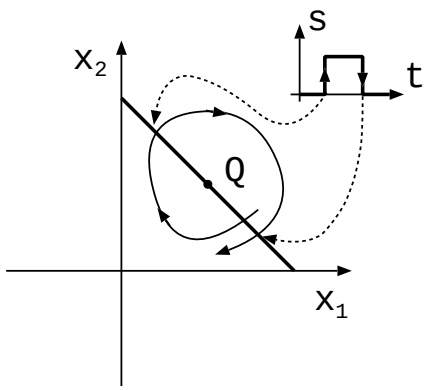

Fig. 2. A sampling pulse $s(t)$ is produced as a (hypothetical) orbit crosses the Poincaré plane (here projected onto the x_1–x_2 plane).

where a hypothetical orbit is shown, projected onto the x_1–x_2 plane, and the edges of the squared waveform $s(t)$ coincide with the times the orbit crosses the plane, which is projected as the line $x_2 = mx_1 + (q_2 - mq_1)$ in Fig. 2. The experimental setup is shown in Fig. 3. The signal $s(t)$ triggers a hold-and-sample device that captures the state variables and transfers the corresponding data to a computer.

2.1. *Circuit implementation*

The schematics is shown in Fig. 4. The Poincaré plane (Σ) is determined by parameters m and Q. The point $Q = (q_1, q_2, 0)$ is set by means

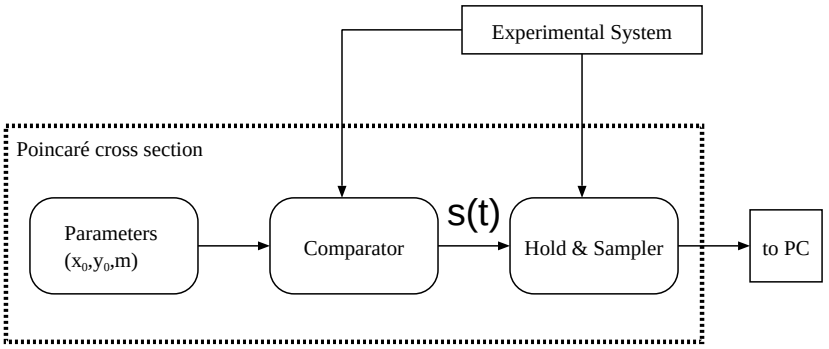

Fig. 3. Experimental setup to collect data at a predefined Poincaré plane.

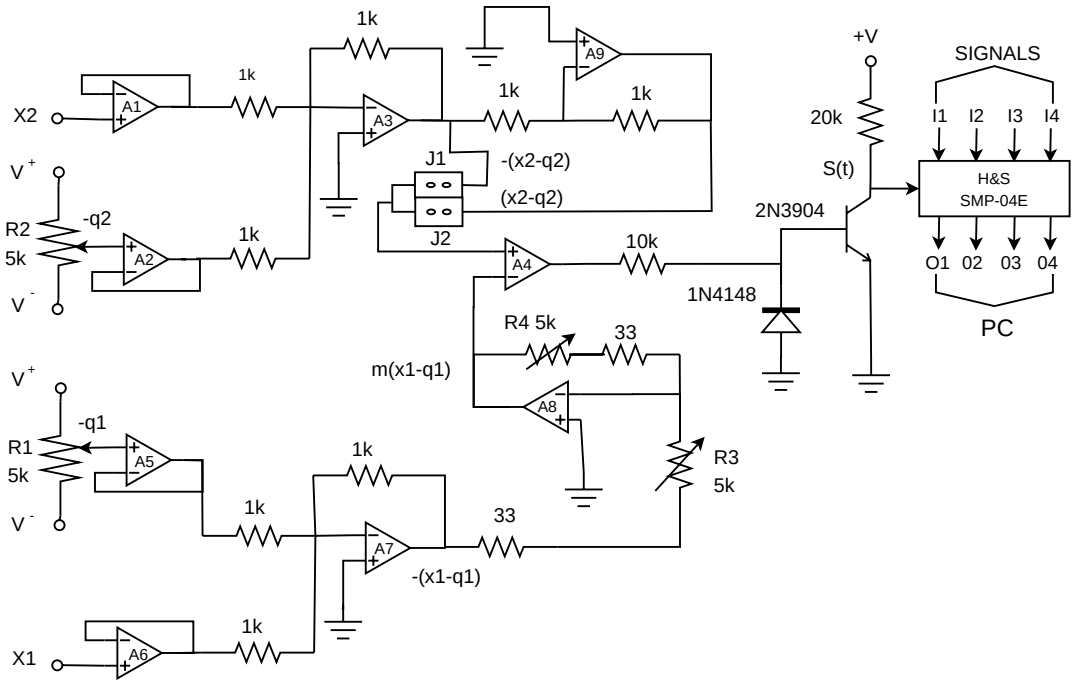

Fig. 4. Schematics of the circuit for Poincaré planes. A plane is defined by three parameters ($q_1(R_1)$, $q_2(R_2)$ and $m(R_3, R_4)$). The coordinates, (x_1, x_2, x_3), of the intersecting point of an orbit with the plane are captured by the H&S device.

of potentiometers R_1 and R_2. Their sliding tabs present the voltage levels $-q_1$ and $-q_2$, through voltage followers A_5 and A_2, to adders configured by amplifiers A_7 and A_3. They yield the outputs $-(x_1(t) - q_1)$ and $-(x_2(t) - q_2)$, where $x_1(t)$, and $x_2(t)$ are state variables of the oscillator. The signal $-(x_1(t) - q_1)$ is then multiplied by constant $-m$ at the output of A_8. Constant m is settled by potentiometers R_3 and R_4 in amplifier A_8. Next, when jumper J1 is open and J2 is closed, amplifier A_4 compares signals $(x_2(t) - q_2)$ and $m(x_1(t) - q_1)$ and the output of A_4 is given adequate levels by transistor T. At the collector pin of T the signal is

$$s(t) = \begin{cases} 5\,\mathrm{V}, & \text{if } x_2(t) > mx_1(t) + (q_2 - mq_1) \\ 0\,\mathrm{V}, & \text{if } x_2(t) < mx_1(t) + (q_2 - mq_1) \end{cases} .$$

The rising edge of signal $s(t)$ triggers the hold-and-sample device (the block H&S in the schematics of Fig. 4) that has the state variables x_1, x_2 and x_3 as inputs. The output levels of H&S are digitized and read by a computer.

When jumpers are reversed from J1-open and J2-closed to J1-closed and J2-open the Poincaré plane is rotated around point Q such that vector $u = (u_1, u_2, 0)$, that is normal to the plane, is flipped to $u' = (u_1, -u_2, 0)$. This provides us with a convenient way of producing wide changes in the plane's orientation during the process of setting the system up.

3. Bifurcations and Induced Maps

The experimental setup described in the previous section is used to follow a cascade of bifurcations and to extract induced maps in a nonlinear oscillator that has a rich variety of attractors [Rulkov, 1996]. The schematics is shown in Fig. 5. It consists of a nonlinear voltage converter (the block labeled N in the schematics) with a linear resonant feedback loop. Chaotic oscillators having this architecture were studied in [Dmitriev *et al.*, 1985]. A minor difference is that we are considering the possibility of externally apply a signal by means of an adder we have interlaced at the input of the nonlinear converter — see Fig. 5. The interested reader will find a detailed description of the oscillator (including the nonlinear converter) in [Rulkov, 1996]. For our discussion it is enough to say that its dynamic evolves in $\mathbb{R}^3$. A point in phase space has coordinates (x_1, x_2, x_3) corresponding to the electric signals indicated in Fig. 5. The two sets of values we used for the electric components (C, C', L, r, and R) and for the gain factor g are listed in the table in Fig. 5.

3.1. *Cascade of bifurcations*

The oscillator in Fig. 5, with set of parameters in the first column of the table, running freely ($\lambda = 0$) has a double-scroll attractor, partially reconstructed from experimental data in Fig. 1. When the oscillator is forced by the external signal $e(t) = \lambda \sin(\omega t)$, at the frequency $f = \omega/2\pi = 2.3\,\mathrm{kHz}$, the attractor follows a rich sequence of bifurcations as the amplitude λ is increased from 0 V, up to 1.6 V.

To follow the cascade of bifurcations, as a function of λ, we defined a Poincaré plane by means of the circuit in Fig. 4. Plane parameters are $q_1 = 80\,\mathrm{mV}$, $q_2 = 1.14\,\mathrm{V}$ and $m = -1.15$. Such a plane is shown in Fig. 1, the attractor corresponds to $\lambda = 0$. The orbits intersect the plane at points $(x_1(t_i), x_2(t_i), x_3(t_i))$ with $x_2(t_i) = mx_1(t_i) + (q_2 - mq_1)$. The times the orbit intersects the Poincaré plane, t_i, $i = 1, 2, \ldots$, are identified by the data acquisition system as the rising edges of signal $s(t)$, provided by the circuit for Poincaré planes, Fig. 4.

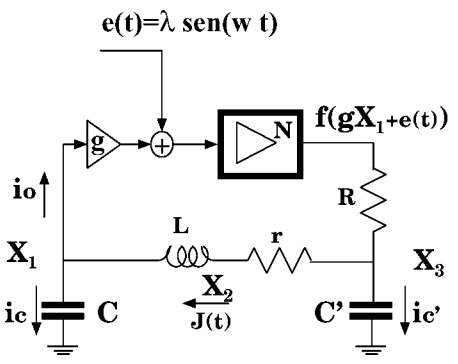

	Logistic Map	Circle Map
C	99.8 nF	0.946 μF
C'	200 nF	1.339 μF
L	26.1 mH	24.26 mH
r	70 Ω	68.9 Ω
R	1139 Ω	1130 Ω
g	1	0.55
λ	0 V	1.2 V
ω	-	2300 Hz

Fig. 5. Schematics of the nonlinear oscillator. Details about the nonlinear converter N can be found in [Rulkov, 1996].

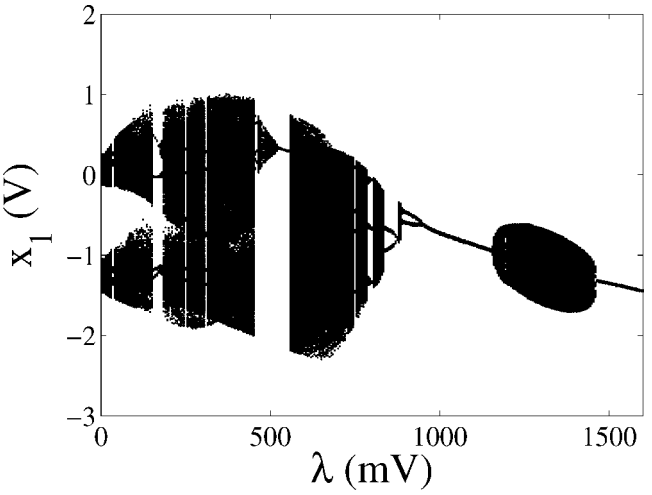

Fig. 6. Cascade of bifurcations. Data was captured with the help of the circuit for Poincaré planes in Fig. 4.

The cascade of bifurcations is shown in Fig. 6. For a fixed value of the amplitude $\lambda \in [0\,\mathrm{V}, 1.6\,\mathrm{V}]$, the set of points in the plot are the values of coordinate $x_1(t_i)$ at times t_i the orbit intersects plane Σ. The following features are worth noticing.

(1) The simplest attractor is a single cycle that manifests in Fig. 6 as a point for the given value of λ. In instances when the values of the amplitude λ range from $\lambda_D = 950\,\mathrm{mV}$ to $\lambda_H = 1150\,\mathrm{mV}$, the oscillator goes around a cycle. By going above $\lambda = \lambda_H$ the cycle becomes a quasiperiodic torus: the oscillator goes through a Hopf–Andronov bifurcation. The width of the torus grows up proportional to $(\lambda - \lambda_H)^{1/2}$. For $\lambda_H < \lambda < 1.4\,\mathrm{v}$ the oscillations are quasiperiodic, around a torus. This case is followed in some detail in Sec. 3.2.1 for the amplitude $\lambda = 1200\,\mathrm{mV}$. At the other end, by going below $\lambda = \lambda_D$ the oscillator goes through a period doubling bifurcation: the simple cycle becomes a double cycle.

(2) A simple cycle is also observed in the cascade in Fig. 6 at values of the amplitude λ in the narrow range from $\lambda_1 = 525\,\mathrm{mV}$ to $\lambda_2 = 555\,\mathrm{mV}$. The bifurcations at these points are of an unknown type. At λ_2 the cycle abruptly becomes a chaotic attractor. By letting the amplitude λ go below λ_1 the cycle becomes a torus whose width grows up *linearly* in $(\lambda_1 - \lambda)$.

(3) Two narrow windows at 250 mV and 310 mV are observed in the cascade of bifurcations, Fig. 6. They correspond to five-fold cycles. The double-scroll nature of the attractor is lost beyond the first window, i.e. for $\lambda > 250\,\mathrm{mV}$.

(4) There is a triple cycle in the window at 800 mV.

3.2. *Induced maps*

3.2.1. *A circle map*

We consider the oscillator with an applied signal $e(t) = \lambda \sin \omega t$ with $\lambda = 1200\,\mathrm{mV}$ and $\omega = 2.3$ kHz. This put us close to the Hopf–Andronov bifurcation point in the cascade of bifurcations in Fig. 6. The analysis of experimental data is simplified by considering the new variables: $x_1'(t) = gx_1(t) + e(t)$, $x_2'(t) = gx_2(t) + \dot{e}(t)$ and $x_3'(t) = gx_3(t)$. The

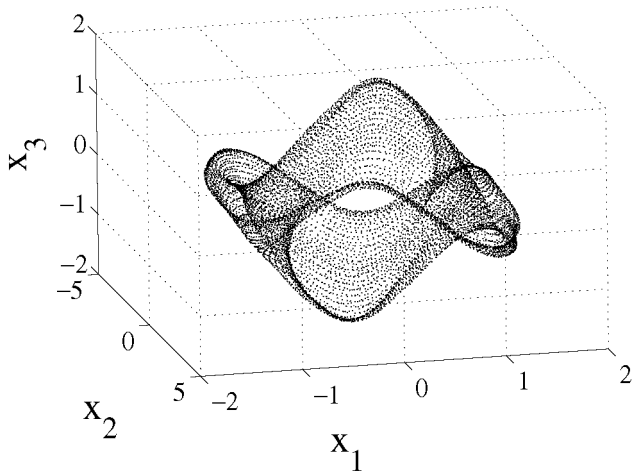

(a)

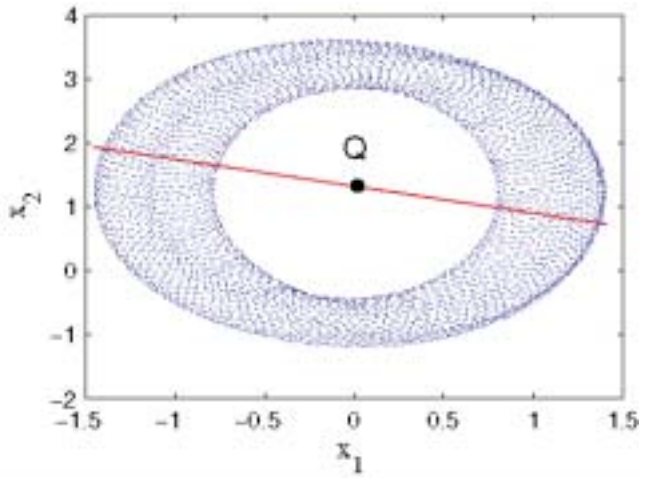

(b)

Fig. 7. (a) Toroidal attractor of the oscillator under a sinusoidal forcing, reconstructed from experimental data. Amplitude and frequency of the external signal are $\lambda = 1200\,\mathrm{mV}$ and $f = 2.3\,\mathrm{kHz}$, respectively. (b) Projection of the attractor onto the x_1–x_2 plane. The line through point Q is the Poincaré plane Σ.

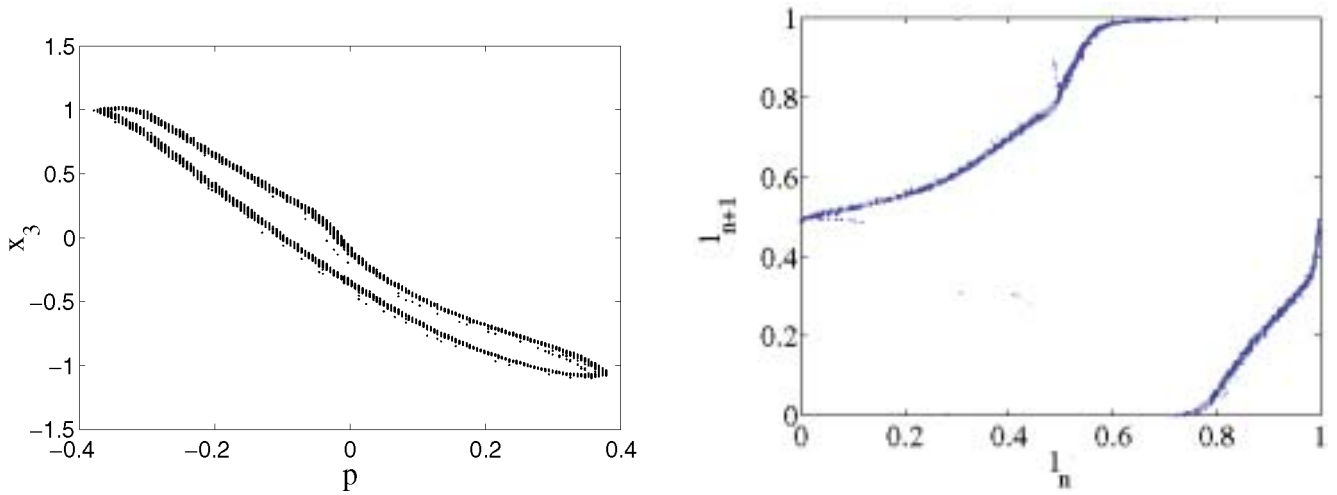

(a) (b)

Fig. 8. (a) Intersection of the toroidal attractor in Fig. 7 with the Poincaré plane Σ. (b) The first return map induced on Σ by the flow, after a homeomorphic deformation of the loop in (a) into the circle S^1.

attractor, in the primed variables, is shown in Fig. 7(a). The projection onto the x_1–x_2 plane is shown in Fig. 7(b). The line passing through point Q is the Poincaré plane Σ, set with the circuit for Poincaré planes, Fig. 4. The state variables are captured by the computer every time the orbit crosses the plane Σ when $\dot{x}_1 > 0$ and $\dot{x}_2 > 0$. The intersection of the attractor with the Poincaré plane, shown in Fig. 8(a), is a closed loop, evidencing that the attractor is a hollow flat torus.

Let $(x_1, x_2)_0, (x_1, x_2)_1, \ldots, (x_1, x_2)_n, \ldots$ be the sequence of points where the orbit intersects the Poincaré plane. The map $(x_1, x_2)_n \mapsto (x_1, x_2)_{n+1}$ induced on the loop by the flow is conjugate to a map of the circle $S^1 = \mathbb{R}/\mathbb{Z}$. Indeed, we have deformed the loop in Fig. 8(a) uniformly into S^1 such that every point $(x_1, x_2)_n$ in the original loop becomes a point p_n in the circle. Then we plotted p_{n+1} versus p_n. The resulting plot is Fig. 8(b), which looks very much like a smooth map of the circle.

Experimental data points distribute around the loop in Fig. 8(a) in a way that is consistent with a quasi-periodic motion of orbits on the torus, having an irrational rotation number. By lifting data in Fig. 8(b) we estimate the rotation number to be around 0.3504 (see, for instance, [Pollicott & Yuri, 1998]).

3.2.2. *The logistic map*

The chaotic oscillator in Fig. 5 has a Rössler type attractor when values of parameters listed in the first column of the table in Fig. 5 are used. The attractor reconstructed from experimental data is shown in Fig. 9(a), projected onto the x_1–x_2 plane. The parameters of the Poincaré plane Σ are all null in this occasion: $m = 0$ and $q_1 = q_2 = 0$. The experimental setup in Fig. 3 was used to collect data at the intersection of plane Σ with the attractor. The plot of the intersection in Fig. 9(b) shows that the attractor is well approximated by a Möbius band (with a gap of unstable orbits in the middle). Thus, the map that is induced by the flow on plane Σ can be considered to be one-dimensional. The state variable x_1 is adequate to describe it. Data in Fig. 9(b) shows that x_1 takes values in the reunion of the intervals P_0 and P_1, shown between brackets in Fig. 9(b). The first return plot, $x_1(n+1)$ versus $x_1(n)$, extracted from experimental data is shown in Fig. 10(a). In this plot we observe that the map transforms P_0 into P_1, and vice versa, and the image of P_0 is just an inverted and uniformly enlarged copy of it. Thus, it is better to consider the second return map. Data is plotted in Fig. 10(b) in the form $x_1(n+2)$ versus $x_1(n)$. Here we see that the original time sequence is decomposed into two subsequences that can be very well approximated, independently, by orbits of surjective logistic maps. Data points in Fig. 10(b) are compared with the graphs of the logistic maps,

$$f_0(x) = 4a_0(x - b_0)\left(1 - \frac{x - b_0}{a_0}\right) + b_0$$

for $x \in P_0$, and

$$f_1(x) = a_1 + b_1 - 4a_1(x - b_1)\left(1 - \frac{x - b_1}{a_1}\right)$$

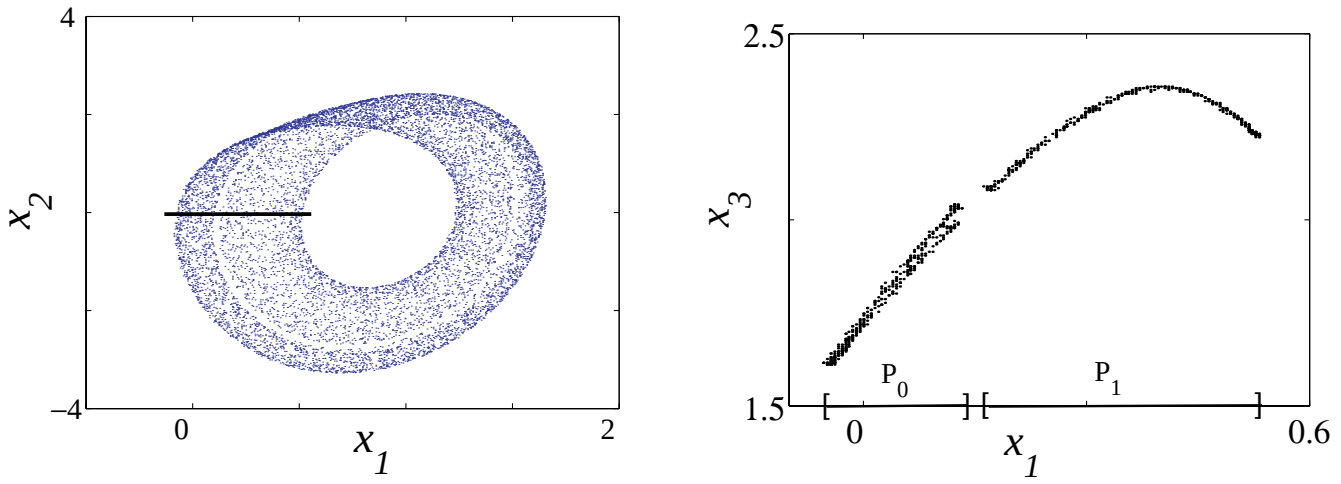

(a) (b)

Fig. 9. (a) Rössler type attractor and Poincaré plane projected onto the x_1–x_2 plane. (b) Intersection of the attractor with the Poincaré plane.

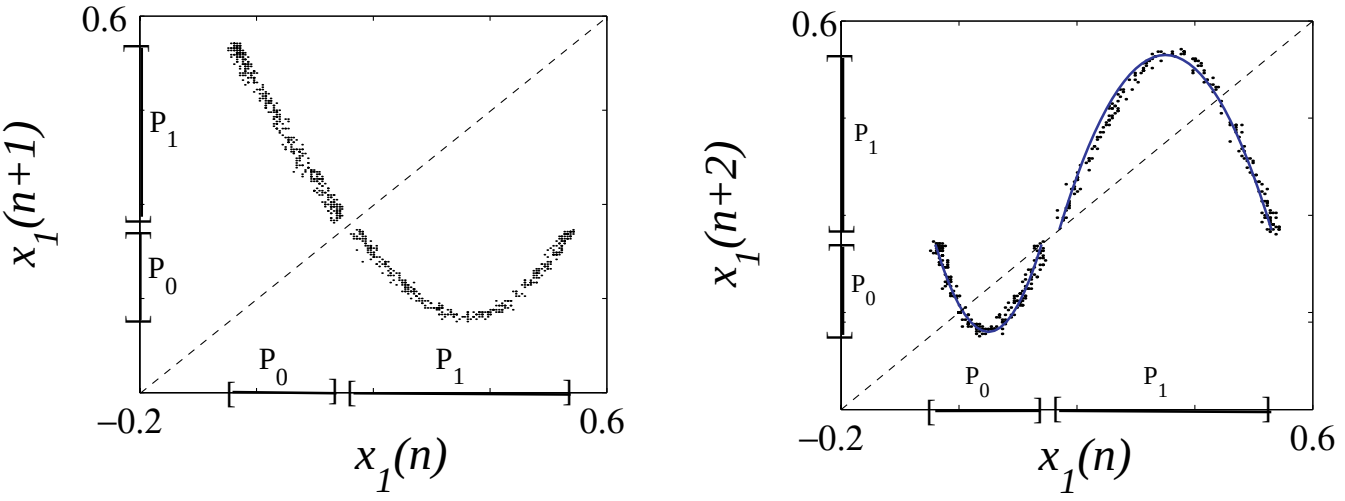

(a) (b)

Fig. 10. (a) First return map in the state variable x_1 that is induced by orbits in the attractor of Fig. 9(a) at the intersections with plane Σ. (b) The second return map. Data points are compared with the graphs of two surjective logistic maps.

for $x \in P_1$. The intervals are $P_0 = [-0.04, 0.14]$ and $P_1 = [0.17, 0.53]$. The parameters for the logistic maps are $a_0 = 0.18$, $b_0 = -0.04$, $a_1 = 0.36$ and $b_1 = -0.17$.

4. Bistable Switching in Chua's Oscillator

The schematics of Chua's oscillator is shown in Fig. 11. If no external signal is applied to the circuit (i.e. $e(t) \equiv 0$), the dynamics is described in a three-dimensional phase space with coordinates ($x := V_1$, $y := V_2$, $z := I_L$) where V_1 and V_2 are the voltage drops across capacitors C_1 and C_2, respectively, and I_L is the current through the inductor L. The oscillator dynamics may either be in a chaotic mode or in a "bistable" mode. The transition between the two "operating modes" is controlled by means of the adjustable resistor R. We selected the bistable regime in which the phase portrait, reconstructed from experimental data in Fig. 12(a), consists of two attracting closed orbits that cycle around each of theunstable fixed points

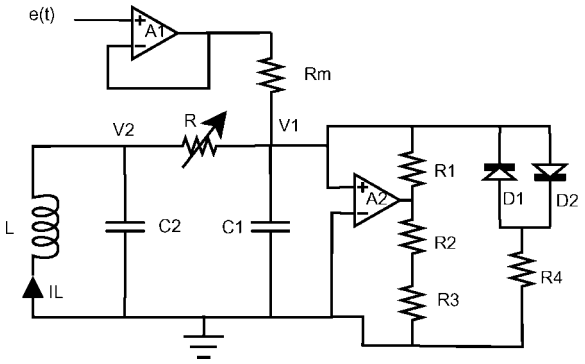

C_1	0.001 μf
C_2	0.01 μf
L	1.676 mHy
R	626 Ω
R_m	12 kΩ
R_1, R_2	220 Ω
R_3	750 Ω
R_4	1.2 kΩ

Fig. 11. Schematics of Chua's oscillator. Component values were selected to get two single closed orbits in phase space. Depending on initial conditions the oscillator goes either around one unstable fixed point or around the other.

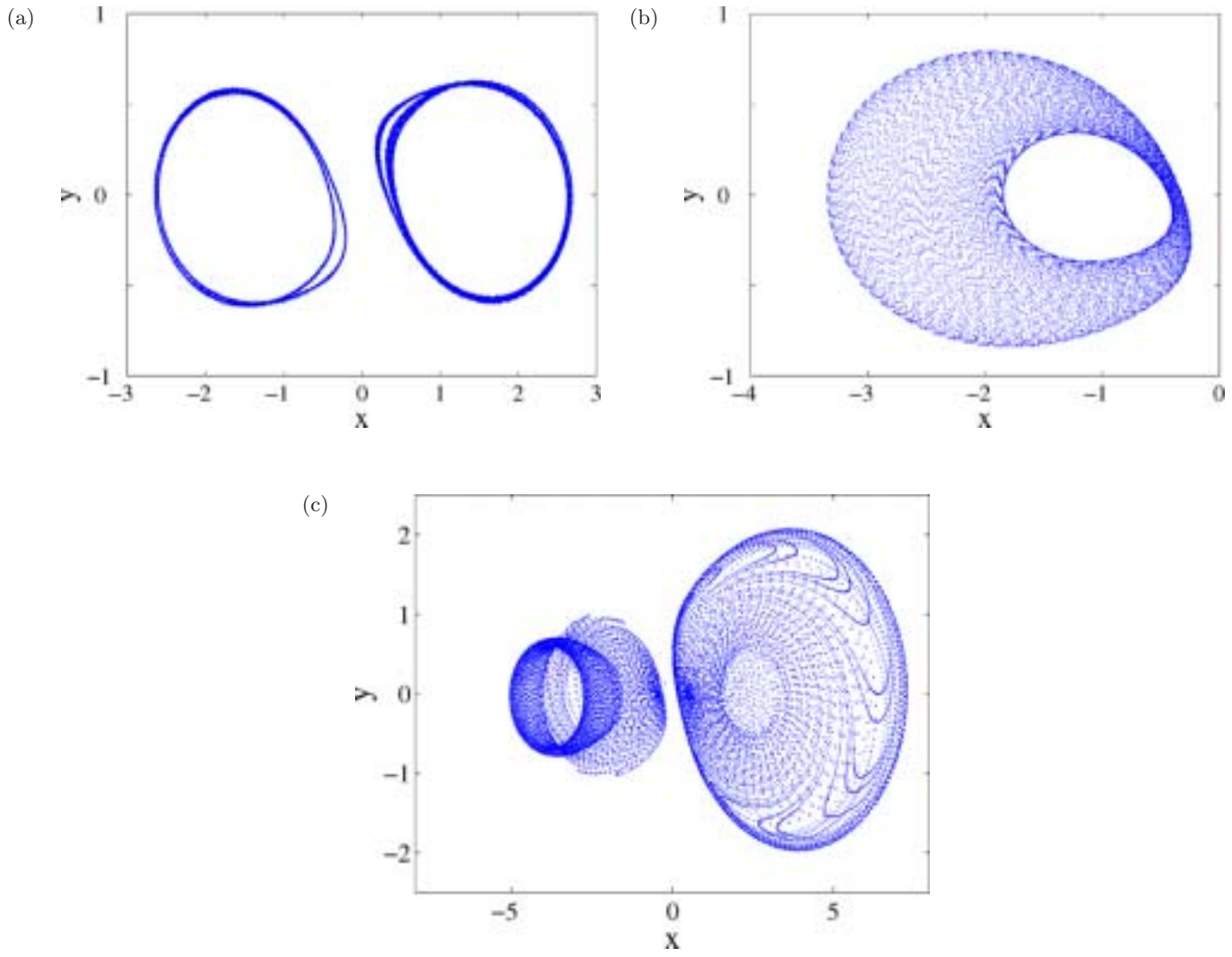

Fig. 12. Phase portrait (projected onto the x–y plane) reconstructed from experimental data from Chua's oscillator in a bistable mode. (a) With no external signal applied the oscillator follows, depending on initial conditions, either of the two closed orbits shown. (b) For an external signal of a small amplitude $\lambda = 1\,\mathrm{V} < \lambda_*$ the orbit is a tightly wounded coil on the $x < 0$ side of phase space. (c) An external signal of amplitude $\lambda = 6.6\,\mathrm{V} > \lambda_*$ forces the point in the orbit to switch between two coils.

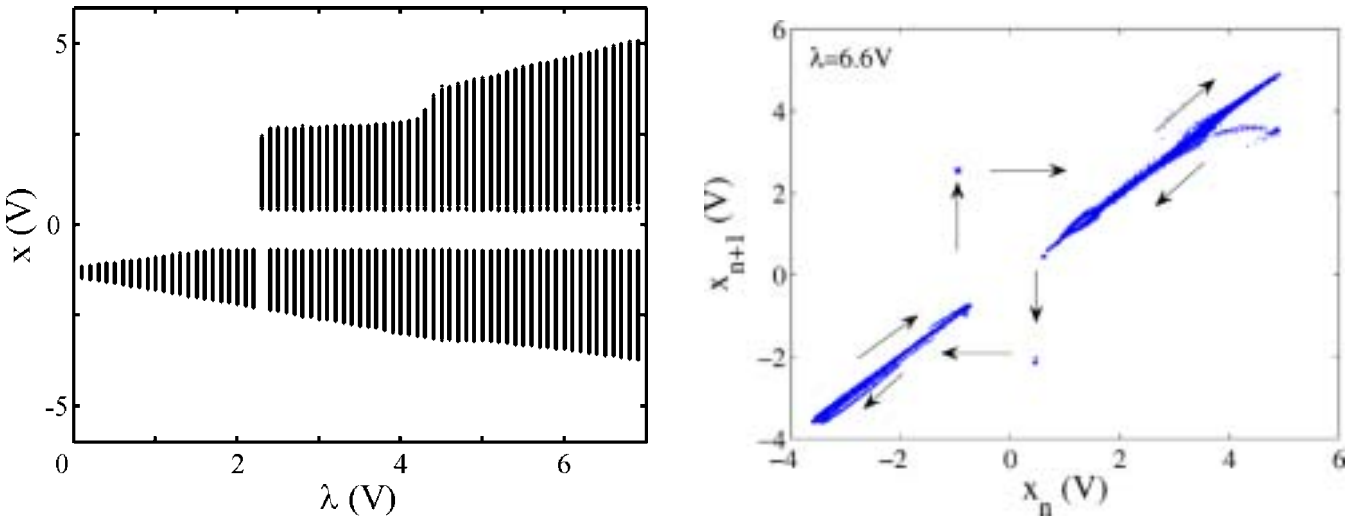

(a) (b)

Fig. 13. Data collected by using the circuit for Poincaré planes. (a) The x-coordinate of the points collected at the intersection of an orbit with the Poincaré plane, for a sequence of values of amplitude λ of the external signal. The threshold for bistable switching is apparent at $\lambda_* = 2.2\,\mathrm{V}$. (b) For $\lambda = 6.6\,\mathrm{V}$ the x-coordinate of the sequence of points is shown in the form of a first-return map. The arrows indicate the way points move in time.

of the oscillator. Depending on the sign of the initial value of coordinate x the orbits are attracted to one of the two closed cycles.

When the oscillator is forced by a sinusoidal external signal $e(t) = \lambda \sin(\omega t)$ of very low frequency ω ($= 2\pi 32\,\mathrm{Hz}$) and a small amplitude λ ($= 1\,\mathrm{V}$), smaller than a certain value λ_* ($= 2.2\,\mathrm{V}$, to be determined below), a point in the orbit in phase space moves along a tightly wounded coil, located on the $x < 0$ side or the $x > 0$ side of phase space, depending on initial conditions. Experimental data for such an orbit is projected onto the x–y plane in Fig. 12(b). When the amplitude λ of the external signal is bigger than the value λ_*, a point in the orbit follows a coil, on the $x < 0$ side of phase space, say, and then jumps to the coil on the other, say $x > 0$, side of phase space. The point keeps switching from coil to coil at a pace that is imposed by the external signal $e(t)$. Both coils, reconstructed from experimental data, are projected onto the x–y plane in Fig. 12(c).

To determine experimentally the threshold λ_* for bistable switching, forced by the external signal, we used the circuit for Poincaré planes to define a plane that intersects the x–y plane along the line $y = -0.42x - 0.1$. At each value of the amplitude λ, in a series of values in the range 0–7 V, successive intersecting points (x_n, y_n, z_n) (in the positive direction $\dot{x} > 0$) of the orbit with the Poincaré plane were collected by the experimental setup. The x-coordinate (x_n) of the collected points are plotted versus λ in Fig. 13(a). The threshold for bistable switching at $\lambda_* = 2.2\,\mathrm{V}$ is apparent in the plot.

Experimental data for the time series $(x_n)_{n\geq 1}$, in the form of a first return plot, is shown in Fig. 13(b).

5. Concluding Remark

We have framed our discussion in a three-dimensional phase space. Circuits for Poincaré planes in phase spaces of dimension greater than three can be constructed following a straightforward extension of the lines we have followed in Sec. 2. That we summarize as follows. Points $x = (x_1, \ldots, x_n) \in \mathbb{R}^n$ that satisfy the condition $(u, x - Q) = 0$ lay in the plane that is perpendicular to vector $u = (u_1, \ldots, u_n)$ and contains point $Q = (q_1, \ldots, q_n) \in \mathbb{R}^n$. The plane is thus defined by

$$(x_1 - q_1) = m_2(x_2 - q_2) + \cdots + m_n(x_n - q_n), \quad (1)$$

where $m_i := u_i/u_1$ (assuming $u_1 \neq 0$), $i = 2, \ldots, n$. The signals on each side of Eq. (1) are passed through a comparator — as we did in amplifier A_4 in Fig. 4 for the signals $x_2(t) - q_2$ and $m(x_1(t) - q_1)$ — to produce the sampling signal $s(t)$.

Acknowledgments

E. Campos-Cantón received financial support from FAI-UASLP under contract C04-FAI-10-30.73. J. S. González is a doctoral fellow of CONACyT in the Graduate Program on Electrical Engineering at UASLP. J. Urías received financial support from CONACyT under contract U–42765–F.

References

Campos, E., Urías, J. & Rulkov, N. [2004] "Multimodal synchronization of chaos," *Chaos* **14**, 48–54.

Diner, S. [1992] "Les voies du chaos déterministe dans l'école russe," *Chaos et Déterminisme*, eds. Dahan Dalmedico, A., Chabert, J.-L. & Chemla, K. (Éditions du Seuil).

Dmitriev, A. S., Kislov, V. Ya. & Starkov, A. O. [1985] "Experimental study of the formation and interaction of strange attractors in a self-excited ring oscillator," *Sov. Phys. Tech. Phys.* **30**, 1439–1440.

Madan, R. N. (ed.) [1993] *Chua's Circuit*: *A Paradigm for Chaos* (World Scientific, Singapore).

Pollicott, M. & Yuri, M. [1998] *Dynamical Systems and Ergodic Theory*, London Mathematical Society, Student Texts 49 (Cambridge University Press).

Rulkov, N. F. [1996] "Images of synchronized chaos: Experiments with circuits," *Chaos* **6**, 262–279.